Solar Energy Materials & Solar Cells 96 (2012) 292–297

Contents lists available at SciVerse ScienceDirect

Solar Energy Materials & Solar Cells

journal homepage: www.elsevier.com/locate/solmat

Letter

Effects of Mg composition on open circuit voltage of Cu_2O–$Mg_xZn_{1-x}O$ heterojunction solar cells

Ziqing Duan [a], Aurelien Du Pasquier [b], Yicheng Lu [a,*], Yi Xu [c], Eric Garfunkel [c]

[a] Department of Electrical and Computer Engineering, Rutgers University, 94 Brett Road, Piscataway, NJ 08854, USA
[b] Department of Materials Science and Engineering, Rutgers University, 671 US Highway 1, North Brunswick, NJ 08902, USA
[c] Department of Chemistry and Chemical Biology, Rutgers University, 610 Taylor Road, Piscataway, NJ 08854, USA

ARTICLE INFO

Article history:
Received 26 May 2011
Received in revised form
13 September 2011
Accepted 17 September 2011
Available online 5 October 2011

Keywords:
Zinc oxide (ZnO)
Cuprous oxide (Cu_2O)
Solar cells
Electrodeposition
MOCVD (metal-organic chemical vapor deposition)

ABSTRACT

$Mg_xZn_{1-x}O$ ($0 \le x \le 0.13$) films grown by metal-organic chemical vapor deposition (MOCVD) were chosen as the n-type semiconductor layer forming a heterojunction with electrodeposited p-type cuprous oxide (Cu_2O) for photovoltaic applications in this study. We investigated the effects of Mg contents (x) on the performance of Ag–Cu_2O–$Mg_xZn_{1-x}O$–fluorine-doped tin oxide (FTO)-glass heterojunction solar cells, where Ag and FTO are used as top and bottom electrodes, respectively. An enhancement of the open-circuit voltage (V_{OC}) with the increase of x, from 251 mV at $x=0$ to 570 mV at $x=10\%$, was observed. In order to understand how V_{OC} increases with Mg%, the band alignment between Cu_2O and $Mg_xZn_{1-x}O$ was demonstrated using X-ray photoelectron spectroscopy (XPS) measurements. The result indicates that the conduction band of $Mg_xZn_{1-x}O$ moves closer to the vacuum level with increasing of x, leading to a decrease of the conduction band offset between $Mg_xZn_{1-x}O$ and Cu_2O and hence an enhancement of theoretical V_{OC}. Another improvement with the increase of Mg% was realized on the shunt resistance (R_{sh}) of devices. With the improved V_{OC} and R_{sh}, a relatively high solar power conversion efficiency ($\eta_{AM1.5}=0.71\%$) was obtained on the $Mg_xZn_{1-x}O$ ($x=10\%$) based solar cell.

1. Introduction

ZnO, a wide bandgap semiconductor (~3.3 eV at room temperature), is also a promising photovoltaic (PV) material when used as an electron acceptor and conductor [1]. It has been demonstrated that n-type ZnO and p-type Cu_2O form heterojunction solar cells, with Cu_2O as the photon absorber [2,3]. A solar conversion efficiency of ~2% was recently reported for Cu_2O–ZnO solar cells [2]; however, it is still one order of magnitude lower than the theoretical limit of Cu_2O solar cells (~20%) [4]. The low solar conversion efficiency of Cu_2O–ZnO solar cells was attributed to the high defect density in polycrystalline Cu_2O thin films and low quality of the Cu_2O–ZnO heterojunction resulted from non-optimal deposition, and inefficient minority carrier transport caused by the planar interface structure [5–9]. Various strategies have been used to improve the solar conversion efficiency (η) of Cu_2O–ZnO heterojunctions, such as using post-deposition cyanide treatment [5], improving the electrical properties of Cu_2O films by optimizing deposition conditions [6,3], refining deposition conditions of the ZnO layers [7,8] and applying a nanowire architecture to the Cu_2O–ZnO interface [9]. In this paper, we report another method to increase the efficiency of Cu_2O–ZnO solar cells using the ternary alloy $Mg_xZn_{1-x}O$ to replace the ZnO, thus, increasing the open circuit voltage V_{OC}.

$Mg_xZn_{1-x}O$, which is formed by alloying MgO with ZnO, has been developed as a promising semiconductor for barrier layers in ZnO/$Mg_xZn_{1-x}O$ quantum wells or superlattices due to its wider bandgap (increasing from 3.3 eV for ZnO up to ~4.0 eV as $x=0.33$ for the direct energy bandgap) [10,11]. It has been observed that the conduction band minimum (CBM) of $Mg_xZn_{1-x}O$ moves closer to the vacuum level with increasing Mg composition x when it forms the heterojunction with other semiconductors such as ZnO [11] and CdS [12]. Olson et al. also found the same trend after they measured the work function of $Mg_xZn_{1-x}O$ films deposited on ITO and saw a decreased work function with increasing Mg composition [13]. They reported that the moving of $Mg_xZn_{1-x}O$ CBM leaded to a reduced conduction band offset and an enhanced V_{OC} in $Mg_xZn_{1-x}O$-P3HT hybrid solar cells. The $Mg_xZn_{1-x}O$ film has also been used as a window layer in Cu(In, Ga)Se_2 solar cells to tune the conduction band offset for higher V_{OC} and efficiency [14,15]. However, there has been no report on the energy band alignment of $Mg_xZn_{1-x}O$ in $Mg_xZn_{1-x}O$–Cu_2O heterojunction. In this paper, we report the band alignment between $Mg_xZn_{1-x}O$ and Cu_2O determined using X-ray photoelectron spectroscopy

* Corresponding author.
E-mail address: ylu@rci.rutgers.edu (Y. Lu).

0927-0248/$ - see front matter © 2011 Elsevier B.V. All rights reserved.
doi:10.1016/j.solmat.2011.09.047

(XPS), from which we investigate the Mg composition effect on the performance of $Mg_xZn_{1-x}O$–Cu_2O heterojunction solar cells.

Cu_2O thin films have been grown by various methods including the thermal oxidation of Cu foils [16], metal-organic chemical vapor deposition (MOCVD) [17], sputtering [18] and electrochemical deposition [19]. Among them, the electrodeposition is the attractive technique because of its ability to use low-cost equipment and chemicals, large area coating and precise control of deposition parameters. In design of the cell structure, the deposition sequence of p-Cu_2O on ZnO films is chosen based on two considerations: first, p-Cu_2O on ZnO shows smaller lattice mismatch than the inverse structure and hence lower density of interface defects and a better solar cell performance [18]; second, this deposition sequence can avoid formation of the impurity phase CuO at the interface that usually occurs in the inverse sequence.

2. Experimental

$Mg_xZn_{1-x}O$ films were grown on $1'' \times 1''$ fluorine-doped tin oxide (FTO)/glass substrates (Pilkington TEC7) by the MOCVD technique at temperature of ~520 °C. Diethylzinc (DEZn) and bis(methylcyclopentadienyl)magnesium (MCp_2Mg) were chosen as the Zn and Mg precursors, respectively. Oxygen gas was used as the oxidizer and injected into the chamber with a separate line to avoid the gas phase reactions. The Mg composition ($0 \le x \le 0.13$) was tuned by changing the precursor flow rate ratio (MCp_2Mg/DEZn). All $Mg_xZn_{1-x}O$ films were kept ~600 nm thick. Cu_2O films were electrodeposited from aqueous solutions of $CuSO_4$ (0.4 mol L^{-1}) and lactic acid (3 mol L^{-1}), with the pH value ~11–12 controlled by NaOH. The working electrode substrates were $Mg_xZn_{1-x}O$/FTO/glass. The counter electrode was a Cu foil. Electrodeposition was performed at a constant voltage of –0.4 V with the bath temperature of 90 °C, under which a growth rate of ~0.2 μm/min was obtained. The thickness of ~4.2–4.5 μm was controlled for all Cu_2O films. Metal contacts (Ag) were then deposited by a Hummer Anatech 6.6 argon plasma sputtering system. Devices were annealed for 15 min at 200 °C in air. Film thickness measurements were performed with a Veeco D150 stylus profilometer. X-ray diffraction (XRD) patterns were acquired on a Siemens D500 X-ray diffractometer. A Hitachi (S-800) field emission scanning electron microscopy (FESEM) was used to check the morphology of Cu_2O and $Mg_xZn_{1-x}O$ films. Hall measurements on the Van der Pauw patterns were conducted to characterize the electrical properties of Cu_2O and $Mg_xZn_{1-x}O$ films. The room temperature transmission spectra of $Mg_xZn_{1-x}O$ films were measured using a UV/vis spectrophotometer (BECKMAN DU 530). The XPS measurements were performed on a XPS spectrometer (Thermo Scientific Inc. K-Alpha) with a monochromatized Al Kα (1486.6 eV) source. *J–V* testing was conducted with an EG&G 273A potentiostat using the full spectrum of a xenon light source shaped with a AM1.5 filter and adjusted to 100 mW/cm^2 with a Newport thermopile. AM1.5 is

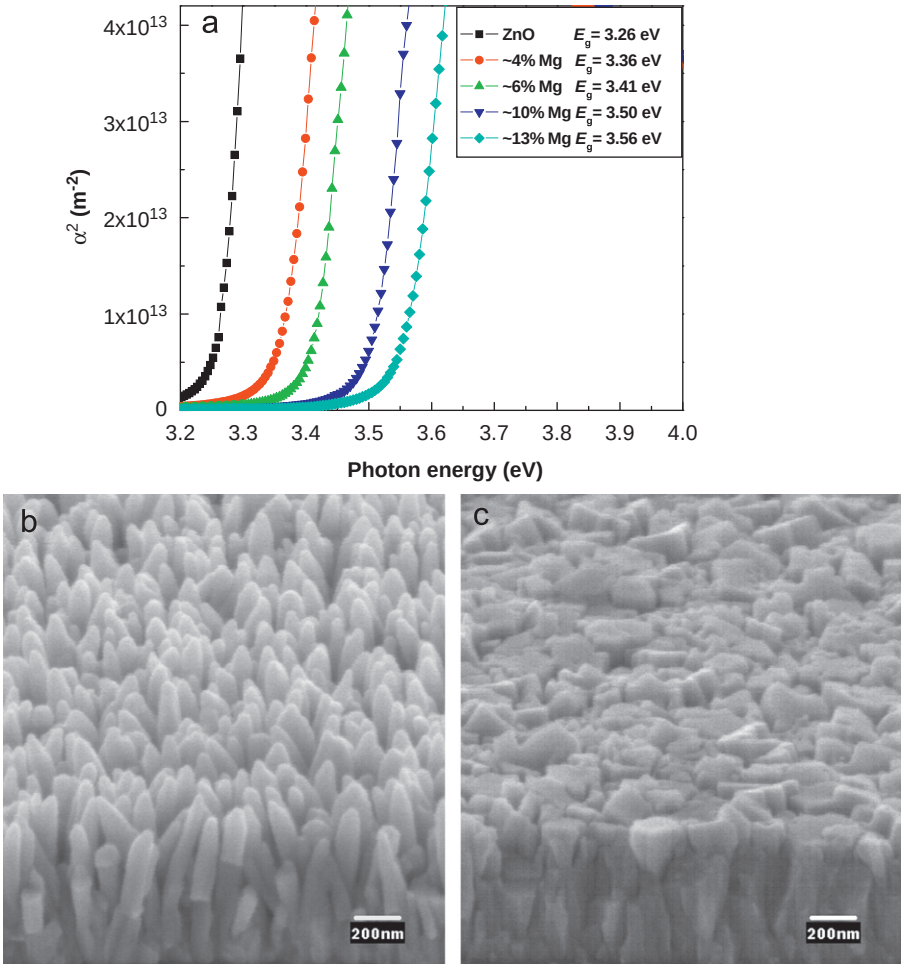

Fig. 1. (**a**) Plots of α^2 versus $h\nu$ for $Mg_xZn_{1-x}O$ ($0 \le x \le 0.13$) films; FESEM images of as-grown $Mg_xZn_{1-x}O$ layers with (**b**) $x=0$ and (c) $x=0.10$.

defined as the incident solar flux at the Earth's surface at incident angle of 37° to the equator, and 100 mW/cm^2 is the power of 1 Sun irradiation under those conditions.

3. Results and discussion

The transmission spectra of $Mg_xZn_{1-x}O$ films were measured at room temperature with a UV–visible spectrophotometer. A transmittance of $>80\%$ in the visible light region is observed on all films, which allows most of the visible light transmitted into the light-absorber layer (Cu_2O) of the solar cell. The bandgap values of $Mg_xZn_{1-x}O$ films are determined by plotting the absorption coefficient α^2 as a function of photon energy ($h\nu$) and fitting these curves to the equation $\alpha = A^*(h\nu - E_g)^{1/2}$, where A^* is a frequency-independent constant, as shown in Fig. 1**a**. Fig. 1**b** and **c** shows the FESEM (field emission scanning electron microscopy) images of as-grown $Mg_xZn_{1-x}O$ with $x=0$ and $x=0.1$, respectively. It is observed that the $Mg_xZn_{1-x}O$ surface morphology evolves with increasing of the Mg composition x. During MOCVD growth, nanostructured ZnO is formed at temperature 400–500 °C [20], resulting from the polarity of ZnO along $\langle 0001 \rangle$ direction. This leads to a high surface energy on {0001} planes [21] and hence a fast growth rate along the c-axis [22]. With the Mg incorporation into ZnO, however, this polarity is weakened, leading to the reduction of the anisotropy of surface energy among all ZnO planes [23]. The growth rates along a- and b-axis would increase, while that along the c-axis decreases. As a result, the morphology of $Mg_xZn_{1-x}O$ changes from sharp nanotip arrays to dense columns with increasing x, as shown in Fig. 1**b** and **c**.

Fig. 2**a** shows the plot of the absorption coefficient α^2 as a function of photon energy ($h\nu$), from which the bandgap of Cu_2O is determined to be 2.0 eV by extrapolating the adsorption edge. Fig. 2**b** shows the dense Cu_2O film (~4.5 μm thick) deposited on $Mg_xZn_{1-x}O$–FTO-glass substrates, taken by FESEM. The XRD pattern of Cu_2O film (Fig. 2**c**) shows the pure Cu_2O phase. None of the other phases, such as CuO or Cu are detected although these two impurities could easily be incorporated into Cu_2O during the deposition process [3]. XPS was used to verify the purity of Cu_2O, as shown in Fig. 2**d.** The Cu $2p_{3/2}$ peak is fit into a single peak at a binding energy of 932.42 eV with a FWHM of 1.27 eV as known from literature values for Cu(I) in Cu_2O [24]. No sub-peak at a binding energy of 933.73 eV, which is attributed to the Cu(II) in CuO, is observed. Moreover, the shake-up satellites peaks that usually appear in CuO and at a binding energy 940 eV–945 eV [25] are not seen in this spectrum. Another possible impurity, Cu, is not easy to quantify by XPS because the Cu $2p_{3/2}$ peak binding energies of Cu(0) and Cu(I) are very close (~0.1 eV difference). But these two states can be distinguished from the Cu LMM-2 Auger transition peak positions, which also appear in photoemission spectra; the peak positions are 568 eV for Cu (metal) and 570 eV for Cu_2O [26]. In our sample, a broad peak centered at 570 eV was found. Although a small peak at 568 eV is possibly buried in the broad peak, it appears that the amount of Cu is negligible.

The current density–voltage (J–V) curves of the heterojunction devices are shown in Fig. 3 and various parameters of the solar cells examined are listed in Table 1. As expected, the V_{OC} value increases with increasing Mg content, from 251 mV for the pure

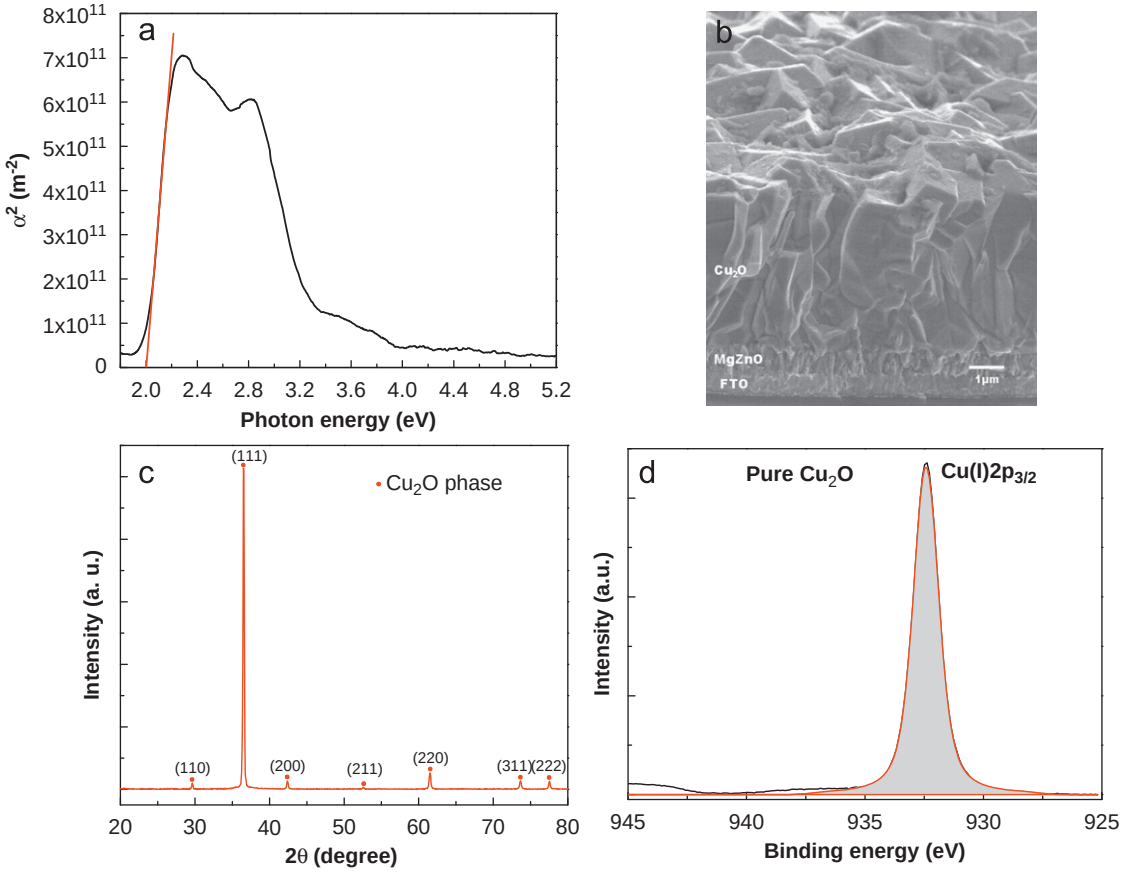

Fig. 2. (**a**) A plot of α^2 versus photon energy ($h\nu$) for the Cu_2O film; (**b**) an FESEM image of the Cu_2O film deposited on $Mg_{0.1}Zn_{0.9}O$–FTO films; (**c**) a typical XRD pattern of the Cu_2O film; (**d**) the Cu $2p_{3/2}$ XPS spectrum from a Cu_2O film.

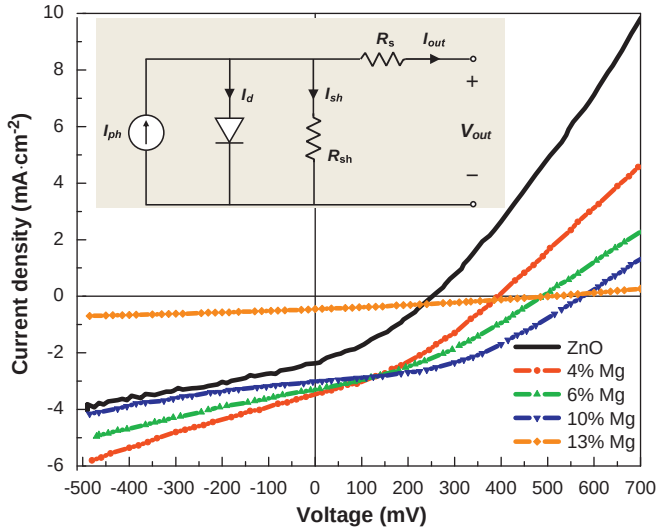

Fig. 3. Current density (J)–voltage (V) characteristics of FTO/$Mg_xZn_{1-x}O$–Cu_2O/Ag solar cells under AM1.5 simulated sunlight. The inset shows the equivalent circuit of the solar cell, where I_{ph}, I_d and I_{sh} are photogenerated current, dark current and shunt current, respectively.

Table 1
Photovoltaic parameters of the FTO/$Mg_xZn_{1-x}O$–Cu_2O/Ag solar cells with different Mg composition x examined under AM1.5 simulated sunlight.

% Mg	η (%)	FF	J_{SC} (mA/cm^2)	V_{OC} (mV)	R_s (Ω cm^2)	R_{sh} (Ω cm^2)
0	0.21	0.34	2.38	251	60	189
4	0.47	0.34	3.44	390	64	223
6	0.57	0.35	3.30	488	91	350
10	0.71	0.42	3.00	575	95	677

ZnO-based device, up to 575 mV for the $Mg_{0.1}Zn_{0.9}O$-based one. In order to understand this enhancement of V_{OC}, we determined the band alignment of Cu_2O and $Mg_xZn_{1-x}O$ using the XPS method proposed by Kraut et al. [27] In this method, the valence band offset (VBO) ΔE_V at the Cu_2O–$Mg_xZn_{1-x}O$ heterojunction interface is given by the following equation:

$$\Delta E_V = (E^{Mg_xZn_{1-x}O}_{Zn2p} - E^{Mg_xZn_{1-x}O}_{V}) - (E^{Cu_2O}_{Cu2p} - E^{Cu_2O}_{V}) - (E^{Mg_xZn_{1-x}O}_{Zn2p}(i) - E^{Cu_2O}_{Cu2p}(i)) \quad (1)$$

where E^B_A refers the binding energy of core level "A" in the sample "B", E^B_V refers the valence band maximum (VBM) and E^B_A (i) represents the binding energy of core level "A" in the sample "B" at the interface. Two heterojunctions of Cu_2O–ZnO and Cu_2O–$Mg_{0.1}Zn_{0.9}O$ were chosen for the XPS measurement. Fig. 4**a** shows the XPS spectra determined from the Cu_2O–ZnO heterojunction. The Cu_2O–$Mg_{0.1}Zn_{0.9}O$ spectra are not shown as they are almost same as that of Cu_2O–ZnO with slightly different binding energy separation values. Based on the XPS data, the corresponding band alignments of Cu_2O–ZnO and Cu_2O–$Mg_{0.1}Zn_{0.9}O$ heterojunctions are schematically drawn as Fig. 4**b**. From that, we can see the VBOs for Cu_2O–ZnO and Cu_2O–$Mg_xZn_{1-x}O$ are 2.73 and 2.77 eV, respectively.The conduction band offsets (CBOs) are determined to be 1.47 eV for Cu_2O–ZnO and 1.27 eV for Cu_2O–$Mg_{0.1}Zn_{0.9}O$. The 0.2 eV difference moves the conduction band of $Mg_{0.1}Zn_{0.9}O$ closer to the vacuum level compared to ZnO; we assume that this change in conduction band edge is responsible for the enhancement of V_{OC}. It is difficult to determine the theoretical V_{OC} from this band alignment without knowing the bulit-in potential V_{bi} determined by the effective work function difference between p and n semiconductors. Assuming that the Fermi level E_{Fn} in n-$Mg_xZn_{1-x}O$ is close to E_{Cn} (CBM in n-$Mg_xZn_{1-x}O$), and E_{Fp} in p-Cu_2O is close to E_{Vp} (VBM in p-Cu_2O) due to the high doping level in both n and p materials, the energy difference between E_{Cn} and E_{Vp} would be approximately equal to the V_{bi}, *i.e.* the upper limit of V_{OC}. With this assumption, the upper limit of theoretical V_{OC} is estimated to be 530 mV for Cu_2O–ZnO and 730 mV for Cu_2O–$Mg_{0.1}Zn_{0.9}O$, respectively.

As shown in the equivalent circuit of the solar cell in the inset of Fig. 3, the low shunt resistance (R_{sh}) could degrade V_{OC} significantly. R_{sh} is generally caused by parallel high-conductivity paths (PHCPs) through the solar cell, or on the edges of the cell. In our case, the interface defects and grain boundaries of both polycrystalline films in the space charge region (SCR) of the heterojunction could act as PHCPs, thus contributing to the R_{sh}. As shown in Table 1, R_{sh} value increases with increasing Mg concentration, from 189 Ω cm^2 for ZnO to 677 Ω cm^2 for $Mg_{0.1}Zn_{0.9}O$, indicate a decrease of the PHCPs with increasing Mg. In addition to the defects contribution, the surface morphology also impacts the PHCP. Figs. 1b and 1c show different surface morphologies between $Mg_xZn_{1-x}O$ (x=0.1) and ZnO (x=0) films, which result in the different effective junction area between $Mg_xZn_{1-x}O$ and Cu_2O. The Cu_2O–ZnO heterojunction have a larger effective junction area than that of the Cu_2O–$Mg_{0.1}Zn_{0.9}O$ cell, due to the nanorods-like surface of ZnO in comparison to the relatively smooth surface of $Mg_{0.1}Zn_{0.9}O$. A larger junction area is favorable for generating more electron/hole pairs, hence a higher photocurrent; however, it would concomitantly possesses more interface defects and grain boundaries. As shown in Table 1, the Cu_2O–ZnO cell has lower R_{sh} due to higher PHCPs than that of Cu_2O–$Mg_{0.1}Zn_{0.9}O$. The lower R_{sh} in Cu_2O–ZnO degrades V_{OC} values (a deviation of 279 mV from the real V_{OC} to the theoretical one) more than that of Cu_2O–$Mg_{0.1}Zn_{0.9}O$ (a deviation of 155 mV).

Unlike the V_{OC} and R_{sh}, the short circuit current density J_{SC} stops being improved and starts to decrease as the Mg percentage increases to over 4%. The resistivity, ρ, of $Mg_xZn_{1-x}O$ films increases with Mg content (x) from ~4 Ω cm (x=0) to ~63 Ω cm for (x=0.1), resulting in increasing in the series resistance R_s (Table 1). With the improved V_{OC} and R_{sh}, the solar conversion efficiency η of devices keep increasing with the increase of Mg content (x) until x=0.1. The highest solar conversion efficiency was obtained on the $Mg_{0.1}Zn_{0.9}O$ sample, $\eta_{AM1.5}$=0.71%, with the J_{SC}=3.0 mA/cm^2 and V_{OC}=575 mV.

A solar cell with a higher Mg content of 13% was also fabricated. However, the electrodeposition of Cu_2O became difficult with a small deposition rate and poor control of film uniformity. The reason could be attributed to the rougher surface morphology and higher resistivity of $Mg_{0.13}Zn_{0.87}O$ films (ρ~78 Ω cm) in comparison with other $Mg_xZn_{1-x}O$ ($x \le 0.1$) films. As consequence, the thickness of as-deposited Cu_2O film was low (~2.5 μm), resulted in lower J_{SC} and detoriated solar cell performances as shown in Fig. 3.

4. Conclusion

In summary, Cu_2O–$Mg_xZn_{1-x}O$ heterojunction solar cells were fabricated on FTO/glass substrates. The effects of Mg composition in $Mg_xZn_{1-x}O$ on the open-circuit voltage of the solar cells were investigated. V_{OC} and $\eta_{AM1.5}$ were enhanced with increasing of Mg content in the $Mg_xZn_{1-x}O$ ($0 \le x \le 0.1$). The solar conversion efficiency $\eta_{AM1.5}$=0.71%, with J_{SC}=3.0 mA/cm^2 and V_{OC}=575 mV were obtained in the Cu_2O–$Mg_{0.1}Zn_{0.9}O$ cell. Further increasing of Mg incorporation (> 10%) would increase the resistivity of $Mg_xZn_{1-x}O$ films and degrade the quality of Cu_2O films made by the electrodeposition, therefore, result in poor cell performance. In order to understand the Mg effect on the enhanced V_{OC}, the band alignment

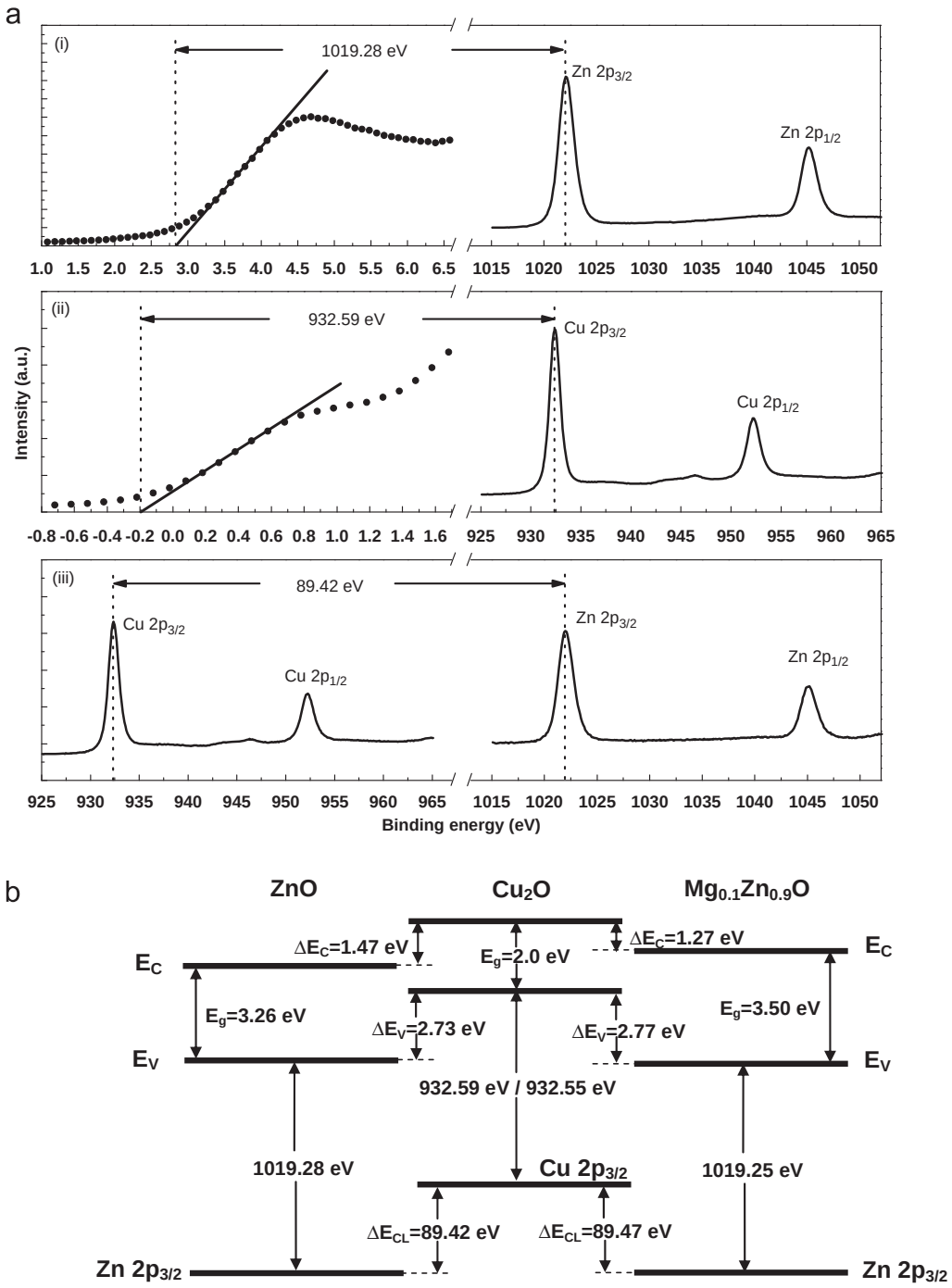

Fig. 4. (**a**) XPS spectra of a Cu_2O–ZnO heterojunction, showing the binding energy separations (i) between the Zn $2p_{3/2}$ core level and the VBM of a bulk ZnO, (ii) between the Cu $2p_{3/2}$ core level and the VBM of a bulk Cu_2O film, and (iii) between the Zn $2p_{3/2}$ and the Cu $2p_{3/2}$ core levels at the heterojunction interface, respectively. (**b**) Schematic of the flat-band diagrams at the heterojunction interfaces determined from the XPS measurements. For simplicity, the Cu_2O–ZnO and Cu_2O–$Mg_{0.1}Zn_{0.9}O$ interfaces are drawn with Cu_2O in the middle.

of Cu_2O–$Mg_xZn_{1-x}O$ heterojunction was measured by XPS. It was found that Mg incorporation into ZnO reduced the conduction band offset between $Mg_xZn_{1-x}O$ and Cu_2O, resulting in an increase of V_{OC}. Furthermore, the Mg incorporation ($0 \le x \le 0.1$) increased the R_{sh}, correspondingly improves V_{OC} value.

Acknowledgements

YL and ZD acknowledge the partial support of the AFOSR DCT grant (FA9550-08-01–0452) and the NSF grant (ECCS-1002178). ADP appreciates the funding from Rutgers TCF and IAMDN. EG and YX acknowledge the support of the NSF.

References

[1] M. Law, L.E. Greene, J.C. Johnson, R. Saykally, P. Yang, Nanowire dye-sensitized solar cells, Nature Materials 4 (2005) 455–459.
[2] A. Mittiga, E. Salza, F. Sarto, M. Tucci, R. Vasanthi, Heterojunction solar cell with 2% efficiency based on a Cu_2O substrate, Applied Physics Letters 88 (2006) 163502-1–163502-3.

[3] M. Izaki, T. Shinagawa, K. Mizuno, Y. Ida, M. Inaba, A. Tasaka, Electrochemically constructed p-Cu_2O/n-ZnO heterojunction diode for photovoltaic device, Journal of Physics D: Applied Physics 40 (2007) 3326–3329.
[4] B.P. Rai, Cu_2O solar cells: a review, Solar Cells 25 (1988) 265–272.
[5] G.K. Paul, R. Ghosh, S.K. Bera, S. Bandyopadhyay, T. Sakurai, K. Akimoto, Deep level transient spectroscopy of cyanide treated polycrystalline p-Cu_2O/n-ZnO solar cell, Chemical Physics Letters 463 (2008) 117–120.
[6] S.S. Jeong, A. Mittiga, E. Salza, A. Masci, S. Passerini, Electrodeposited ZnO/Cu_2O heterojunction solar cells, Electrochimica Acta 53 (2008) 2226–2231.
[7] T. Minami, T. Miyata, K. Ihara, Y. Minamino, S. Tsukada, Effect of ZnO film deposition methods on the photovoltaic properties of ZnO–Cu_2O heterojunction devices, Thin Solid Films 494 (2006) 47–52.
[8] H. Tanaka, T. Shimakawa, T. Miyata, H. Sato, T. Minami, Electrical and optical properties of TCO–Cu_2O heterojunction devices, Thin Solid Films 244 (469–470) (2004) 80–85.
[9] K.P. Musselman, A. Wisnet, D.C. Iza, H.C. Hesse, C. Scheu, J.L. MacManus-Driscoll, L. Schmidt-Mende, Strong efficiency improvements in ultra-low-cost inorganic nanowire solar cells, Advanced Materials 22 (2010) E254–E258.
[10] A. Ohtomo, M. Kawasaki, T. Koida, K. Masubuchi, H. Koinuma, Y. Sakurai, Y. Yoshida, T. Yasuda, Y. Segawa, $Mg_xZn_{1-x}O$ as a II–VI widegap semiconductor alloy, Applied Physics Letters 72 (1998) 2466–2468.
[11] A. Ohtomo, M. Kawasaki, I. Ohkubo, H. Koinuma, T. Yasuda, Y. Segawa, Structure and optical properties of ZnO/$Mg_{0.2}Zn_{0.8}O$ superlattices, Applied Physics Letters 75 (1999) 980–982.
[12] G.V. Rao, F. Säuberlich, A. Llein, Influence of Mg content on the band alignment at CdS/(Zn,Mg)O interfaces, Applied Physics Letters 87 (2005) 032101-1–032101-3.
[13] D.C. Olson, S.E. Shaheen, M.S. William, J.M. Maikel, F.A.M.V. Hest, R.T. Collins, D.S. Ginley, Band-offset engineering for enhanced open-circuit voltage in polymer-oxide hybrid solar cells, Advanced Functional Materials 17 (2007) 264–269.
[14] T. Minemoto, Y. Hashimoto, W. Shams-Kolahi, T. Satoh, T. Negami, H. Takakura, Y. Hamakawa, Control of conduction band offset in wide-gap Cu(In,Ga)Se_2 solar cells, Solar Energy Materials and Solar Cells 75 (2003) 121–126.
[15] F.Y. Meng, Y. Chiba, A. Yamada, M. Konagai, Growth of $Zn_{1-x}Mg_xO$ films with single wurtzite structure by MOCVD process and their application to Cu(InGa)$(SSe)_2$ solar cells, Solar Energy Materials and Solar Cells 91 (2007) 1887–1891.
[16] N.A. Mohemmed Shanid, M. Abdul Khadar, Evolution of nanostructure, phase transition and band gap tailoring in oxidized Cu thin films, Thin Solid Films 516 (2008) 6245–6252.
[17] G.G. Condorelli, G. Malandrino, I. Fragala, Metal-organic chemical vapor deposition of copper-containing phases: kinetics and reaction mechanisms, Chemistry of Materials 6 (1994) 1861–1866.
[18] K. Akimoto, S. Ishizuka, M. Yanagita, Y. Nawa, G.K. Paul, T. Sakurai, Thin film deposition of Cu_2O and application for solar cells, Solar Energy 80 (2006) 715–722.
[19] P.E. De Jongh, D. Vanmaekelbergh, J.J. Kelly, Cu_2O: electrodeposition and characterization, Chemistry of Materials 11 (1999) 3512–3517.
[20] S. Muthukumar, H. Sheng, J. Zhong, Z. Zhang, N.W. Emanaetoglu, Y. Lu, Selective MOCVD growth of ZnO nanotips, IEEE Transactions on Nanotechnology 2 (2003) 50–54.
[21] P.W. Tasker, The stability of ionic crystal surfaces, Journal of Physics C: Solid State Physics 12 (1979) 4977–4984.
[22] W. Li, E. Shi, W. Zhong, Z. Yin, Growth mechanism and growth habit of oxide crystals, Journal of Crystal Growth 203 (1999) 186–196.
[23] M. Kim, Y. Hong, J. Yoo, G. Yi, G. Park, K. Kong, H. Chang, Surface morphology and growth mechanism of catalyst-free ZnO and $Mg_xZn_{1-x}O$ nanorods, Physica Status Solidi RPL (2) (2008) 197–199.
[24] J.P. Tobin, W. Hirschwald, J. Cunningham, XPS and XAES studies of transient enhancement of Cu^1 at CuO surfaces during vacuum outgassing, Applied Surface Science 16 (1983) 441–452.
[25] P.E. Larson, X-ray induced photoelectron and auger spectra of Cu, CuO, Cu_2O, and Cu_2S thin films, Journal of Electron Spectroscopy and Related Phenomena 4 (1974) 213–218.
[26] T. Ghodselahi, M.A. Vesaghi, A. Shafiekhani, A. Baghizadeh, M. Lameii, XPS study of the Cu@Cu_2O core-shell nanoparticles, Applied Surface Science 255 (2008) 2730–2734.
[27] E.A. Kraut, R.W. Grant, J.R. Waldrop, S.P. Kowalczyk, Precise determination of the valence-band edge in X-ray photoemission spectra: application to measurement of semiconductor interface potentials, Physical Review Letters 44 (1980) 1620–1623.